

Received June 20, 2019, accepted June 30, 2019, date of publication July 8, 2019, date of current version July 25, 2019.

Digital Object Identifier 10.1109/ACCESS.2019.2927158

# Fast Blind Image Deblurring Using Smoothing-Enhancing Regularizer

ZEYANG DOU<sup>ID</sup>, KUN GAO<sup>ID</sup>, XIAODIAN ZHANG, AND HONG WANG<sup>ID</sup>

Key Laboratory of Photoelectronic Imaging Technology and System, Ministry of Education of China, Beijing Institute of Technology, Beijing 100081, China

Corresponding author: Kun Gao (gaokun@bit.edu.cn)

This work was supported in part by the National Natural Science Foundation of China under Grant 61875013 and Grant 61827814, and in part by the Special Project of the Science and Technology Ministry of China under Grant 2017YFF0107102.

**ABSTRACT** Blind deconvolution is a highly ill-posed problem for the restoration of degraded images and requires prior knowledge or regularization. Recently, various priors have been proposed and the models based on these priors have achieved state-of-the-art performances. In this paper, we present a blind image deblurring method based on a computationally efficient and effective image regularizer. The proposed regularizer is motivated by the fact that the success of recent priors mainly stems from their properties, which implicitly generate an unnatural latent image suppressing insignificant structures and preserving only salient edges. These salient edges guide the models to estimate an accurate kernel. In this paper, the proposed regularizer termed smoothing-enhancing regularizer, not only assures that only salient structures in the image are preserved but also enhances these salient structures to help the model estimate the more accurate kernel. To efficiently solve the proposed model, we develop an efficient numerical approach based on the half-quadratic splitting algorithm and the lagged-fixed-point iteration scheme. The optimization scheme only requires a few additional shrinkage operations compared with the original half-quadratic splitting algorithm, making our method much faster than recent leading methods. The qualitative and quantitative experimental results show that our algorithm achieves the state-of-the-art results and can be extended to other challenging deblurring tasks, such as those involving text, face, and low-illuminated images. Furthermore, the proposed method is much more computationally efficient than the recent state-of-the-art algorithms with up to more than 10× faster execution time.

**INDEX TERMS** Blind restoration, motion blur, half quadratic splitting, smoothing-enhancing regularizer.

## I. INTRODUCTION

Blind image deblurring is designed to estimate a blur kernel and simultaneously recover a sharp image from a blurred one. This is a problem in classical computer science that has received considerable attention in recent years. Blind image deblurring is vital to improve the qualities of blurry image and video sources. It is used to further improve various multimedia processing tasks such as image analysis [6] and surveillance video analysis [7]. The demand for deblurring continues to increase drastically as evermore photos are taken using hand-held cameras and smartphones. As camera shake is often inevitable and difficult to reproduce, it is challenging to remove blur from a single image.

The associate editor coordinating the review of this manuscript and approving it for publication was Michele Nappi.

When the blur is spatially invariant and uniform, the blur process can be modeled as follows:

$$f = k * u + n \quad (1)$$

where  $f$ ,  $k$ ,  $u$ , and  $n$  are the blur image, blur kernel, true sharp image, and noise respectively, and  $*$  is the convolution operator. Since only  $f$  is known in most cases, we need to simultaneously recover both the true sharp images and the blur kernels. This problem is highly ill-posed because there are more unknown variables than known ones. Therefore, it is necessary to incorporate additional information about the most likely latent sharp image  $u$  and kernel  $k$  into this model. This additional information is called prior in Bayesian statistical inference or regularizer in inverse problems.

Recent research has focused on developing efficient and robust priors for latent sharp images. For instance, many researchers [8]–[10] have used sparse gradient priors to

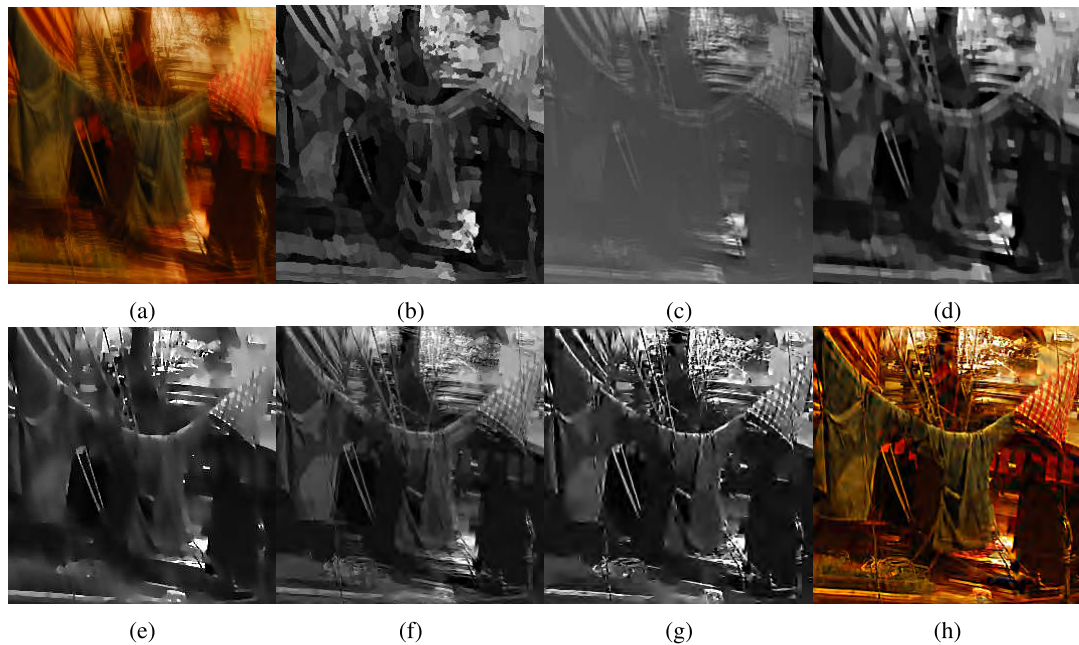


**FIGURE 1.** Intermediate unnatural latent images exist in many state-of-the-art approaches. (a) Blurry image, (b) Cho's method [1], (c) Normalized sparsity [2], (d) Shan et al. [3], (e)  $L_0$  prior [4], (f) dark channel prior [5], (g) Proposed, (h) Final result by the proposed method.

model latent sharp images. However, as Freeman et al. [11] have shown, deblurring methods based on this prior have a counter-intuitive flaw: the prior incurs lower cost with blurred images than sharp images. To solve this problem, a number of alternatives have been used, including explicit strong edge-selection methods [1], [12]–[17] and implicit special regularization methods [2], [4], [5], [18]. Cho and Lee [1] explicitly selected strong edges and used the shock filter [19] to create step reference edges for kernel estimation. Xu and Jia [12] extended this method by detecting and using large-scale edges for kernel estimation. These two models have been extensively validated in natural image motion deblurring, but they are not suitable for the specific deblurring tasks, such as deblurring face images. Natural image priors that favor clean images to blurred ones have also been recently introduced, including the normalized sparsity regularization [2],  $L_0$ -based prior [4], dark channel prior [5], extreme channel prior [20], multi-scale structure prior [21], reweighted graph total variation prior [22], class-adapted image prior [23], and the prior learned from a large dataset [18]. Recently, deep learning has been applied in image deblurring as well. Hrabiš et al. [24] proposed an convolutional neural network (CNN) to deblur text images. Schuler et al. [25] proposed a deep network to directly estimate the blur kernel and then adopt a nonblind deconvolution approach to recover the latent sharp image. Chakrabarti [26] trained a deep network to predict the Fourier coefficient of a deconvolution filter. **However, the performances of deep learning based models on blind image deblurring [27], [28] still show inferior results compared with conventional optimization-based approaches on**

**handling large blur kernels** [18]. Li et al. [18] took advantage of both conventional MAP-based framework and the discriminative learning ability of deep CNNs to blindly deblur images.

Despite the different appearances of above methods, most of them share the commonness during the intermediate steps: they generate unnatural latent images containing only salient image structures [4]. As shown in Fig. 1, the generated latent images are very different from natural ones, containing only large edges and high-contrast structures while suppressing others. These unnatural latent images are vital for kernel estimation. However, most of the recent priors generate these unnatural images by suppressing the small details and leaving the blurry large edges unchanged. For example, Shan et al. [3] uses a large smooth weight to suppress insignificant structures and a small weight to preserve strong ones; the normalized sparsity prior smooths the latent image in similar ways by treating the  $L_2$ -norm of image gradients as smooth weights in iterations; the  $L_0$  prior removes harmful subtle image structures and leaves the blurry strong edges unchanged. As can be seen from Fig. 1(c)–1(e), the strong edges generated by these priors are not as sharp as those in the clean image. Though the dark channel prior favors the clean images, it doesn't directly impact the edges, thus it may enhance the harmful subtle image structures and create the false edges, as shown in Fig. 1(f).

A natural idea is if the high-contrast edges were properly enhanced, the kernel estimation process would obviously benefit from these enhanced high contrast edges. In this paper, we propose a new image regularizer, termed

smoothing-enhancing regularizer, that not only removes the harmful subtle image structures but also enhances the high contrast ones of the unnatural latent images. One example is shown in Fig. 1(g). Different from most of existing methods, our approach elegantly incorporates the smoothing and enhancing operations into one regularizer. Compared to explicit strong edge-selection methods which usually use local shock filter to enhance the strong edges, our strong edges are selected and adaptively enhanced without filtering in extra steps.

The proposed regularizer is challenging to optimize owing to its highly nonlinear nature. We thus derive a fast optimization scheme based on half-quadratic splitting and fixed-point iteration scheme. The optimization scheme is quick because it only requires a few additional shrinkage operations. Owing to the high efficiency of the optimization scheme, the proposed method is much more efficient than recent leading algorithms [5], [20] and [18], with up to more than  $10\times$  faster execution time. The proposed algorithm archives the state of the art results on natural deblurring natural images and can be extended to other challenging deblurring tasks, such as text, face, and low illuminated images.

The contributions of this work are as follows:

(1) We propose a simple yet effective image regularizer that can simultaneously suppress small details and enhance strong edges.

(2) We derive an efficient optimization scheme to minimize the highly nonlinear objective function, which is more than  $10\times$  faster than recent leading algorithms.

(3) Our algorithm achieves highly competitive performance on natural image deblurring tasks. Our model also works well on other specific tasks, such as the deblurring of text, face and low-illumination images.

## II. SMOOTHING-ENHANCING REGULARIZER

Given an input image  $u$ , the proposed regularizer  $\phi(D)$  is given by:

$$\phi(D) = \int \frac{D(x, y)}{D^2(x, y) + \varepsilon} dxdy \quad (2)$$

where

$$D(x, y) = \sqrt{u_x^2(x, y) + u_y^2(x, y)} \quad (3)$$

$u_x$  and  $u_y$  are partial derivatives of  $u$  along the  $x$  and  $y$  directions respectively, and  $\varepsilon$  is a positive constant.

The regularizer  $\phi(\cdot)$  has different penalty properties from existing regularizers. Fig. 2 shows the shapes of different regularizer losses. We see that when the gradient magnitude  $D(x, y)$  is below some threshold, minimizing  $\phi(D)$  pushes  $D$  to zero because the cost decreases with  $D$ . However, when the gradient magnitude is above the threshold,  $\phi(\cdot)$  assigns a lower penalty to larger  $D$ , which means that the edge is enhanced. With this different shape,  $\phi(\cdot)$  simultaneously smooths small structures and enhances strong edges based on the gradient magnitude. Fig. 3 illustrates a family of  $\phi$  with  $\varepsilon \subseteq \{10^{-1}, 10^{-2}, 10^{-3}\}$ . We see that smaller values of  $\varepsilon$  leads

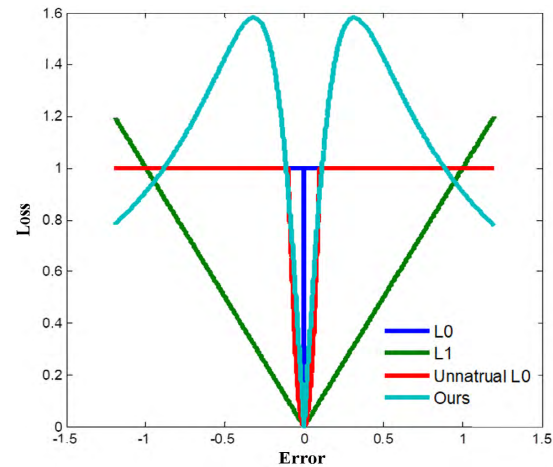


FIGURE 2. Plots of different regularizers.

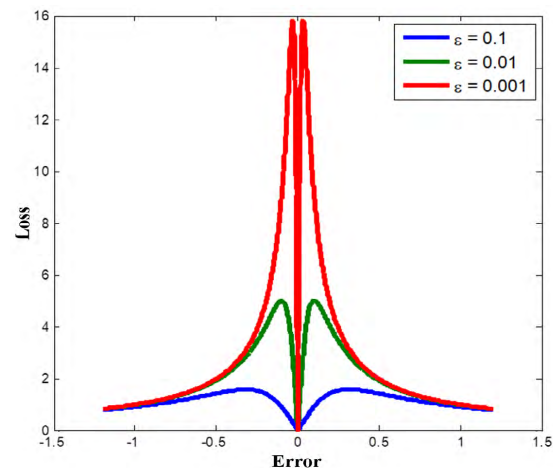


FIGURE 3. Shapes of the proposed regularizers with different  $\varepsilon$ .

to sharper peaks of  $\phi$ , resulting in more aggressively sharpen effect.

To better understand how the proposed regularizer works, we recall total variation (TV) [29]–[31], which is an edge preserving smoothing regularizer. Given an input image, the isotropic TV is:

$$TV(u) = \int D(x, y) dxdy \quad (4)$$

We use  $D$  to denote  $D(x, y)$  for notation simplicity. We can derive the associated heat flow of (4) as follows. First, we give  $u$  a small perturbation  $\lambda\delta u$ ,  $\delta u|_{\partial\Omega} = 0$ . The Gateaux differential  $\delta TV$  is

$$\begin{aligned} \delta TV &= \int \left\{ \frac{d}{d\lambda} (\sqrt{(u_x + \lambda\delta u_x)^2 + (u_y + \lambda\delta u_y)^2}) dxdy \right\} \Big|_{\lambda=0} \\ &= \int \frac{u_x \delta u_x + u_y \delta u_y}{\sqrt{u_x^2 + u_y^2}} dxdy \\ &= \int \frac{\nabla u \cdot \nabla \delta u}{D} dxdy \end{aligned} \quad (5)$$

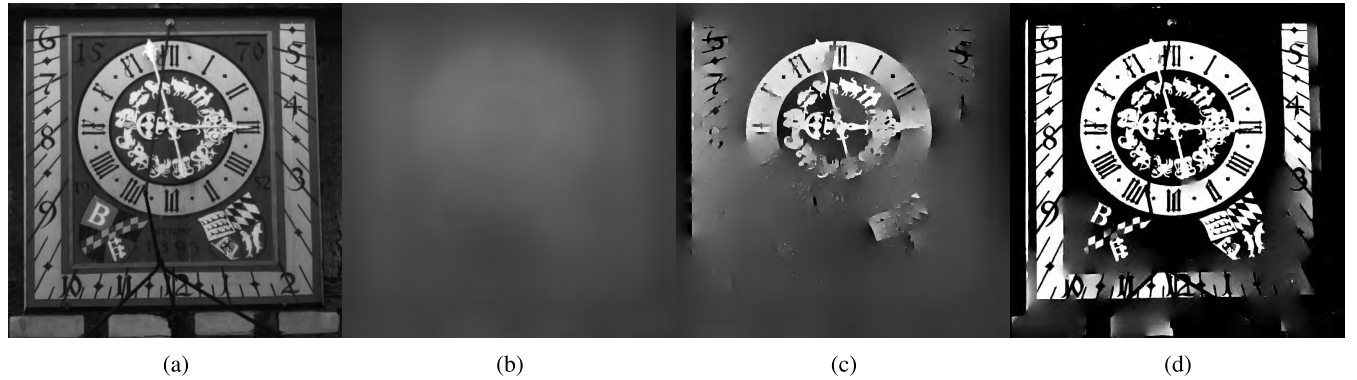


**FIGURE 4.** The filtered images of a gray-scale input with different  $\varepsilon$ . (a) Original image, (b)  $\varepsilon = 0.5$ , (c)  $\varepsilon = 0.05$ , (d)  $\varepsilon = 0.01$ .

where  $\nabla$  is the gradient operator, and  $\cdot$  is inner product operator. Thanks to Green's formula

$$\int_{\Omega} v \cdot \nabla u dx = - \int_{\Omega} u \nabla \cdot v dx + \int_{\partial\Omega} v u ds \quad (6)$$

where  $\nabla \cdot$  is the divergence operator, we have

$$\int \frac{\nabla u \cdot \nabla \delta u}{D} dxdy = - \int \delta u \nabla \cdot \left( \frac{\nabla u}{D} \right) dxdy + \int \frac{\nabla u}{D} \delta u ds \quad (7)$$

Because  $\delta u|_{\partial\Omega} = 0$ , we have

$$\int_{\partial\Omega} \frac{\nabla u}{D} \delta u ds = 0, \quad (8)$$

Thus,

$$\int \frac{\nabla u \cdot \nabla \delta u}{D} dxdy = - \int \delta u \nabla \cdot \left( \frac{\nabla u}{D} \right) dxdy. \quad (9)$$

Thus, the Gateaux derivative is

$$TV' = -\nabla \cdot \left( \frac{\nabla u}{D} \right) \quad (10)$$

Finally, the associated heat flow is

$$\frac{\partial TV}{\partial t} = \nabla \cdot \left( \frac{1}{D} \nabla u \right) \quad (11)$$

where  $t$  represents time. As  $D$  is always nonnegative, the diffusion coefficient  $\frac{1}{D}$  is non-negative as well, indicating that (11) is a smoothing partial differential equation (PDE). If the diffusion coefficient is negative, (11) becomes an enhancing PDE, which enhance edges with the number of iterations. This is the key to understanding the proposed regularizer. Formally, we have the following proposition for the proposed regularizer.

- *Proposition 1:* Given  $\varepsilon > 0$ , if  $D^2(x_0, y_0) < \varepsilon$ , minimizing  $\phi(D)$  is equivalent to smoothing the small structures; otherwise minimizing  $\phi(D)$  is equivalent to sharpening the strong edges.



**FIGURE 5.** Smoothing results using original and hard thresholding regularizer. (a) Original image, (b) original regularizer, (c) hard thresholding regularizer.

*Proof:* Based on the similar derivation of the TV regularizer, the associated heat flow of (2) is:

$$\frac{\partial \phi}{\partial t} = \nabla \cdot \left( \frac{(\varepsilon - D^2)}{(D^2 + \varepsilon)^2 D} \nabla u \right) \quad (12)$$

If  $D^2 \leq \varepsilon$ , the diffusion coefficient is non-negative and (12) is a smoothing PDE; if  $D^2 > \varepsilon$ , the diffusion coefficient at  $(x_0, y_0)$  is negative, (12) is an enhancing PDE.

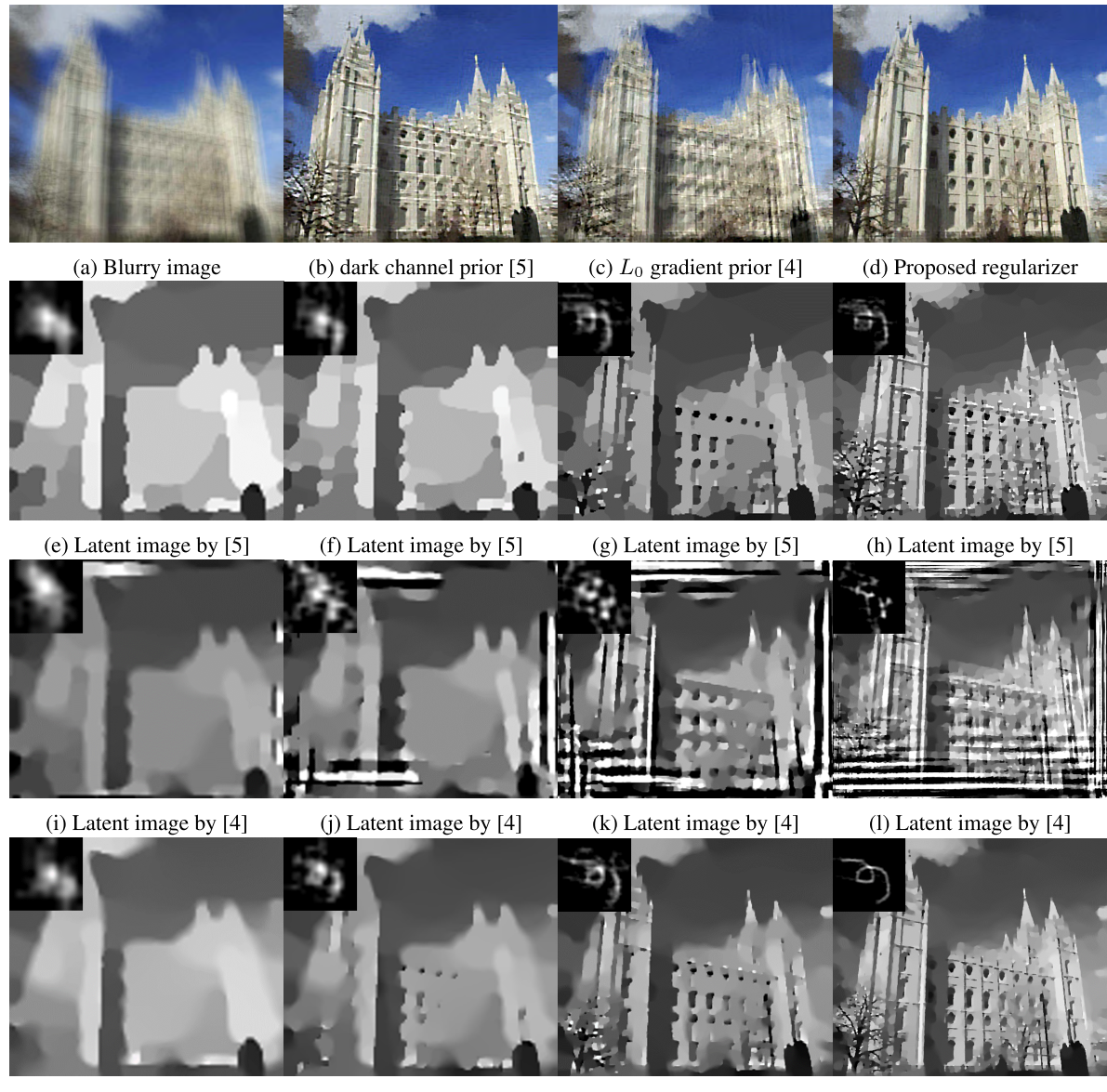
Proposition 1 shows that  $\varepsilon$  plays a key role for smoothing and enhancing. It is a gradient-norm threshold which determines whether the structure is smoothed or enhanced. Fig. 4 shows an example of the smoothing-enhancing regularizer with various set of  $\varepsilon$ . From the figure we see that smaller  $\varepsilon$  remove less subtle structures and enhance more high-contrast structures.

### III. MODEL AND OPTIMIZATION

#### A. FRAMEWORK

Based on our analysis, we use the smoothing-enhancing regularizer to seek the unnatural latent image containing sharpened strong edges. In this paper, we use grayscale images to estimate kernels. For color images, we transform them into grayscale images. Given a blurry image  $\mathbf{f} \in \mathbb{R}^{HW}$  where  $H$  and  $W$  are height and width respectively, our discrete objective function is:

$$\min_{\mathbf{u}, \mathbf{k}} : E(\mathbf{u}, \mathbf{k}) = \|\mathbf{K}\mathbf{u} - \mathbf{f}\|_2^2 + \alpha \mathbf{1} \cdot \frac{\mathbf{D}}{\mathbf{D}^2 + \varepsilon} + \gamma \|\mathbf{k}\|_2^2 \quad (13)$$



(m) Latent image by proposed (n) Latent image by proposed (o) Latent image by proposed (p) Latent image by proposed

**FIGURE 6. Unnatural intermediate images and deblurred results of different methods. First row: Input Blurry image deblurred results of [4], [5] and the proposed method; Second row: Intermediate images by dark channel prior [5]; Third row: Intermediate images by  $L_0$  gradient prior [4]; Fourth row: Intermediate images by proposed regularizer.**

subject to the constraints

$$\mathbf{k} \geq 0, \quad \mathbf{1} \cdot \mathbf{k} = 1 \quad (14)$$

where  $\mathbf{K}$  represents the block circulant matrix with circulant block formed by  $\mathbf{k}$ ,  $\mathbf{u}$ ,  $\mathbf{k}$  and  $\mathbf{D}$  are the vectors formed by corresponding variables with lexicographical column ordering.  $\mathbf{1}$  is the vector with all elements filled with 1, and  $\cdot$  represents the inner product operator.  $\alpha$  and  $\gamma$  are the regularization parameters.

The above function has three terms. The first is the fidelity term enforcing the blur model constraint, the second term is the smoothing-enhancing regularizer, which is instrumental to guiding kernel estimation, and the third term helps suppress

kernel noise. The constraints on  $\mathbf{k}$  follow from the nature of the blur formation. The regularization weights control the strength of the kernel and image regularizer.

## B. OPTIMIZATION

Equation (13) can be minimized by alternatively solving

$$\mathbf{u}^{i+1} = \arg \min_{\mathbf{u}} \|\mathbf{K}^i \mathbf{u} - \mathbf{f}\|_2^2 + \alpha \mathbf{1} \cdot \frac{\mathbf{D}}{\mathbf{D}^2 + \varepsilon} \quad (15)$$

$$\mathbf{k}^{i+1} = \arg \min_{\mathbf{k}} \|\mathbf{U}^{i+1} \mathbf{k} - \mathbf{f}\|_2^2 + \gamma \|\mathbf{k}\|_2^2 \quad (16)$$

subject to the constraints (14).  $\mathbf{U}$  is a block circulant matrix with circulant block formed by  $\mathbf{u}$ . Following previous work [32], [33], we estimate blur kernels in a coarse-to-fine

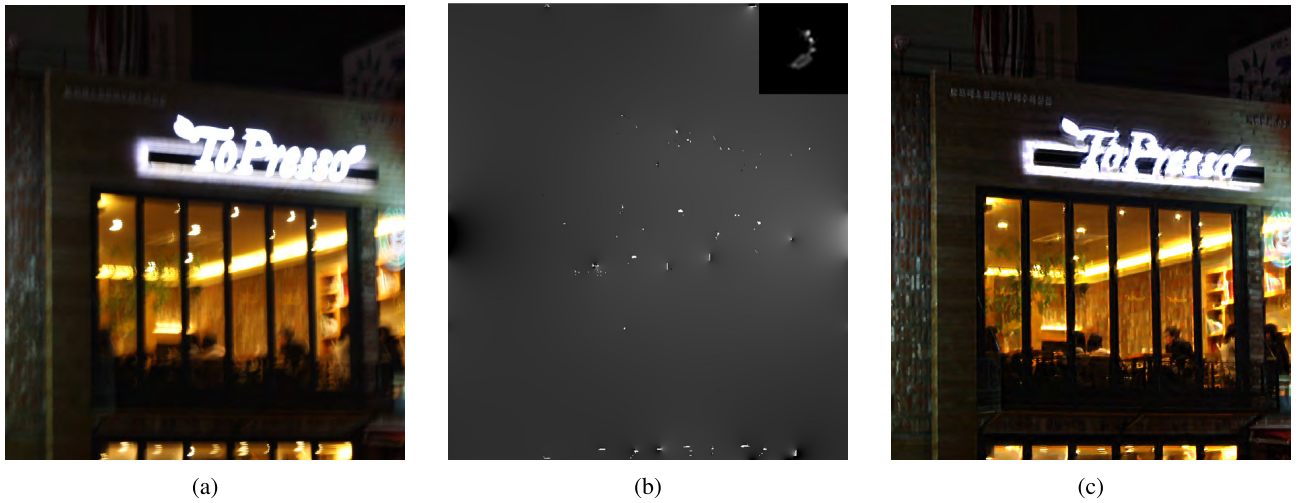


**FIGURE 7.** Latent image and deblurring result on a challenging low-light image. (a) Blurry image; (b) Latent image; (c) Deblurred image.

framework, i.e., an upsampled estimated  $k$  from the previous level is taken to initialize the next one. To recover more details, we gradually reduce  $\alpha$  in the computation.

### 1) ESTIMATING THE LATENT IMAGE $u$

Minimizing (15) is challenging because the objective function is non-convex and the smoothing-enhancing regularizer is highly nonlinear. Based on the half-quadratic splitting minimization method [4], [34], we propose an effective method to solve it. We introduce a dual variable  $\mathbf{b} = (\mathbf{b}_x, \mathbf{b}_y)$  to replace  $\nabla u = (u_x, u_y)$ . The objective function can then be rewritten as

$$\begin{aligned} \min_{\mathbf{u}, \mathbf{b}} : & ||\mathbf{K}^i \mathbf{u} - \mathbf{f}||_2^2 + \alpha \mathbf{1} \cdot \frac{\sqrt{\mathbf{b}_x^2 + \mathbf{b}_y^2}}{\mathbf{b}_x^2 + \mathbf{b}_y^2 + \varepsilon} \\ & + \frac{\beta}{2} (||\mathbf{b}_x - \mathbf{u}_x||_2^2 + ||\mathbf{b}_y - \mathbf{u}_y||_2^2) \end{aligned} \quad (17)$$

Note that the smoothing-enhancing regularizer is decoupled from (15) in this way. When  $\beta$  is close to  $\infty$ , the solution of (17) converges to that of (15). The new objective function (17) can be effectively minimized by solving the following problems alternatively.

$$\min_{\mathbf{b}} : \alpha \mathbf{1} \cdot \frac{\sqrt{\mathbf{b}_x^2 + \mathbf{b}_y^2}}{\mathbf{b}_x^2 + \mathbf{b}_y^2 + \varepsilon} + \frac{\beta}{2} (||\mathbf{b}_x - \mathbf{u}_x||_2^2 + ||\mathbf{b}_y - \mathbf{u}_y||_2^2) \quad (18)$$

$$\min_{\mathbf{u}} : ||\mathbf{K}^i \mathbf{u} - \mathbf{f}||_2^2 + \frac{\beta}{2} (||\mathbf{b}_x - \mathbf{u}_x||_2^2 + ||\mathbf{b}_y - \mathbf{u}_y||_2^2) \quad (19)$$

Minimizing (18) is equivalent to solving the following equation system:

$$\begin{aligned} \alpha \frac{(\varepsilon - \mathbf{b}_x^2 - \mathbf{b}_y^2) \mathbf{b}_x}{(\mathbf{b}_x^2 + \mathbf{b}_y^2 + \varepsilon)^2 \sqrt{\mathbf{b}_x^2 + \mathbf{b}_y^2}} + \frac{\beta}{2} (\mathbf{b}_x - \mathbf{u}_x) &= 0 \\ \alpha \frac{(\varepsilon - \mathbf{b}_x^2 - \mathbf{b}_y^2) \mathbf{b}_y}{(\mathbf{b}_x^2 + \mathbf{b}_y^2 + \varepsilon)^2 \sqrt{\mathbf{b}_x^2 + \mathbf{b}_y^2}} + \frac{\beta}{2} (\mathbf{b}_y - \mathbf{u}_y) &= 0 \end{aligned} \quad (20)$$

Note that equation system (20) cannot be solved explicitly. However, if we lag  $(\varepsilon - \mathbf{b}_x^2 - \mathbf{b}_y^2)/(\mathbf{b}_x^2 + \mathbf{b}_y^2 + \varepsilon)^2$  behind one iteration, the equation system (20) has a closed-form solution using the shrinkage operator. The iteration scheme of (20) is summarized as algorithm 1. We can adopt the stopping criteria by setting a threshold  $\tau$  for  $||\mathbf{b}_x^i - \mathbf{b}_x^{i-1}||_2 + ||\mathbf{b}_y^i - \mathbf{b}_y^{i-1}||_2$ , i.e.,  $||\mathbf{b}_x^i - \mathbf{b}_x^{i-1}||_2 + ||\mathbf{b}_y^i - \mathbf{b}_y^{i-1}||_2 < \tau$ . In practice, however, we find 5 iterations are enough. Thus, in this paper we empirically set the max iteration to 5 as a trade-off between accuracy and speed.

#### Algorithm 1 Fix Point Iteration Algorithm

Initialize  $\mathbf{b} = (\mathbf{u}_x, \mathbf{u}_y)$

For  $k = 1 : 5$

$$\begin{aligned} \mathbf{b}_x^{k+1} &= \max(0, 1 - \frac{\alpha}{\beta} \frac{\varepsilon - \mathbf{b}_x^k - \mathbf{b}_y^k}{(\mathbf{b}_x^k + \mathbf{b}_y^k + \varepsilon)^2 \sqrt{\mathbf{u}_x^2 + \mathbf{u}_y^2}}) \mathbf{u}_x \\ \mathbf{b}_y^{k+1} &= \max(0, 1 - \frac{\alpha}{\beta} \frac{\varepsilon - \mathbf{b}_x^k - \mathbf{b}_y^k}{(\mathbf{b}_x^k + \mathbf{b}_y^k + \varepsilon)^2 \sqrt{\mathbf{u}_x^2 + \mathbf{u}_y^2}}) \mathbf{u}_y \end{aligned} \quad (21)$$

End

Equation (21) indicates that if the elements in  $\mathbf{b}_x^2 + \mathbf{b}_y^2 > \varepsilon$ , the optimal  $\mathbf{b}_x$  and  $\mathbf{b}_y$  are greater than  $\mathbf{u}_x$  and  $\mathbf{u}_y$ , respectively, leading to edge enhancement; otherwise they result in structural smoothness.

Given  $\mathbf{b}$ , (19) is a quadratic minimization problem with the following closed form solution

$$\mathbf{u}^{i+1} = F^{-1} \left( \frac{\bar{F}(\mathbf{k}^i)F(\mathbf{f}) - \beta F(\nabla^T \mathbf{b}^{i+1})}{|F(\mathbf{k}^i)|^2 - \beta F(\Delta)} \right) \quad (22)$$

where  $F$  and  $F^{-1}$  denote the Fast Fourier Transform (FFT) and inverse FFT respectively, and  $\bar{F}$ ,  $\nabla^T$  and  $\Delta$  are the conjugate FFT, divergence and Laplace operator matrix, respectively. Note that the proposed algorithm can be integrated into

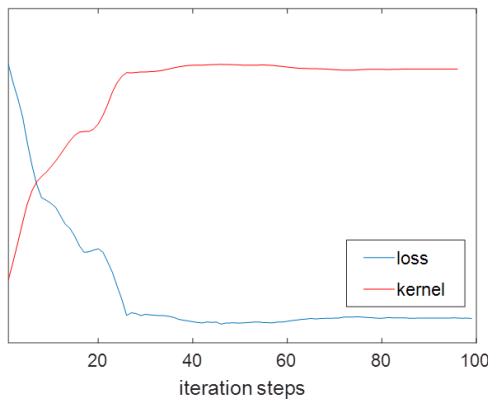


**FIGURE 8.** Convergence illustration of loss and kernel similarity.

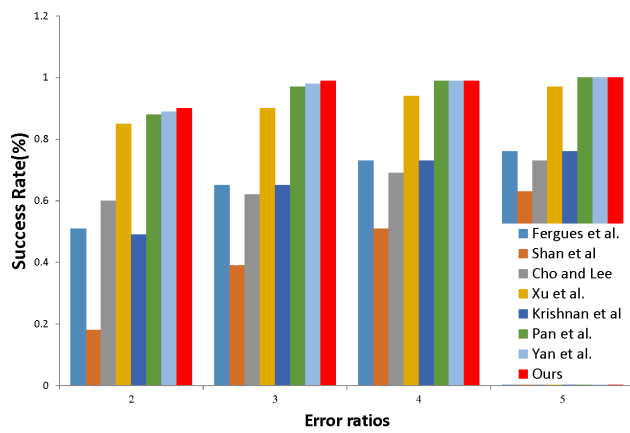


**FIGURE 9.** Quantitative evaluations on benchmark dataset [11].

other optimization frameworks such as Alternating Direction Method of Multipliers (ADMM) [38] and split Bregman method [39] as well.

As discussed in the introduction, the subtle image structures are harmful to kernel estimation, thus the unnatural latent images are expected to contain only high-contrast structures. Note that  $\mathbf{b}_x$  and  $\mathbf{b}_y$  are actually the targets for  $\mathbf{u}_x$  and  $\mathbf{u}_y$ , hence we can easily remove the subtle image structures via hard thresholding. Specifically, having computed  $\mathbf{b}_x$  and  $\mathbf{b}_y$  using Algorithm 1, we set the corresponding elements of  $\mathbf{b}$  to zero if  $\sqrt{\mathbf{b}_x^2 + \mathbf{b}_y^2}$  is less than some iterative threshold  $\lambda$ . Fig. 5 shows comparisons of the original and hard thresholding regularizers. Algorithm 2 summarizes the main steps for solving (17).

## 2) ESTIMATING THE BLUR KERNEL

Given  $\mathbf{u}^{i+1}$ , the kernel estimation in (16) is a quadratic optimization problem with a closed form solution in frequency domain. The solution is expressed as

$$\mathbf{k}^{i+1} = F^{-1}\left(\frac{\bar{F}(\mathbf{u}^{i+1})F(\mathbf{f})}{|F(\mathbf{u}^{i+1})|^2 + \gamma}\right) \quad (23)$$

---

### Algorithm 2 Main Steps for Solving (17)

```

Input:  $\mathbf{K}, \mathbf{f}, \alpha, \beta, \varepsilon, \lambda, \mathbf{b}_x, \mathbf{b}_y = \mathbf{u}_x, \mathbf{u}_y, \beta_{max}, \mathbf{u} = \mathbf{f}$ 
While  $\beta < \beta_{max}$  do
    Solve  $\mathbf{b}$  using Algorithm 1.
     $\mathbf{b}(\sqrt{\mathbf{b}_x^2 + \mathbf{b}_y^2} < \lambda) = 0$ .
    Solve  $u$  using (22).
     $\beta = 2\beta$ .
     $\lambda = \frac{\lambda}{2}$ .
End While
Output: Intermediate Latent Image  $u$ .
```

---

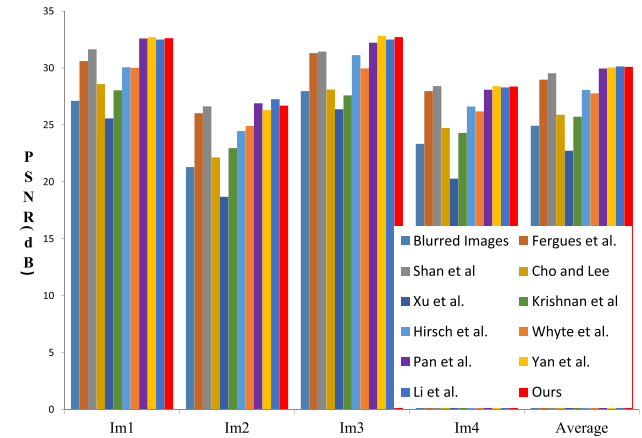


**FIGURE 10.** Quantitative evaluations on benchmark dataset [35].

Note that all multiplication and division operators are element-wise. After recovering the kernel at each level, we add constraint (14) to meet the nature of blur formation.

## 3) FINAL IMAGE RESTORATION

Once the kernel  $\mathbf{k}$  for the finest level is obtained, numerous non-blind deconvolution algorithms can be used to recover the final clear image from  $\mathbf{f}$ . As we focus on kernel estimation, we use the non-blind deconvolution algorithm [32] to recover the final sharp image with the estimated kernel. Algorithm 3 outlines the main steps of our approach.

---

### Algorithm 3 Overall Algorithm

```

Input: blurred image  $\mathbf{f}$  and kernel initial guess  $\mathbf{k}^0$ 
```

Loop over coarse-to-fine levels

for  $i = 1 : 5$  do

Solve  $\mathbf{u}$  using Algorithm 2;

Solve  $\mathbf{k}$  using (23), (14);

$\alpha = \frac{\alpha}{1.1}$ ;

end

Interpolate  $\mathbf{k}$  to finer level as initialization

end

Non-blind image restoration

---

**Output:** Final Recovered image



**FIGURE 11.** Visual comparisons using one challenging image form the benchmark dataset [35]. (a) Blurry image; (b) Krishnan [2]; (c) Yan [20]; (d) Li [18]; (e) Proposed. (Best viewed on high-resolution display with zoom-in).

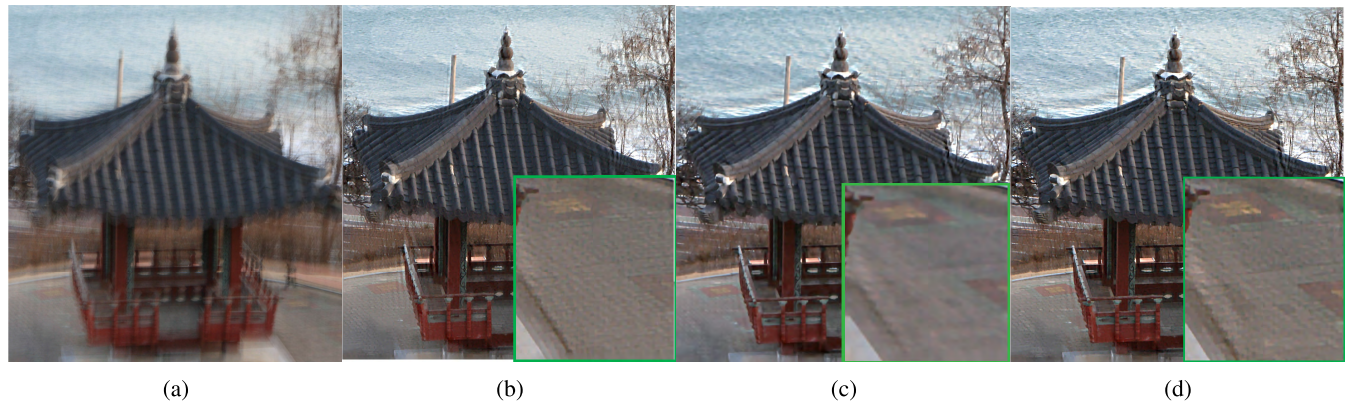


**FIGURE 12.** Visual comparisons of state-of-the-art methods on real world blurry image. (a) Blurry image; (b) Pan [5]; (c) Yan [20]; (d) proposed. (Best viewed on high-resolution display with zoom-in).

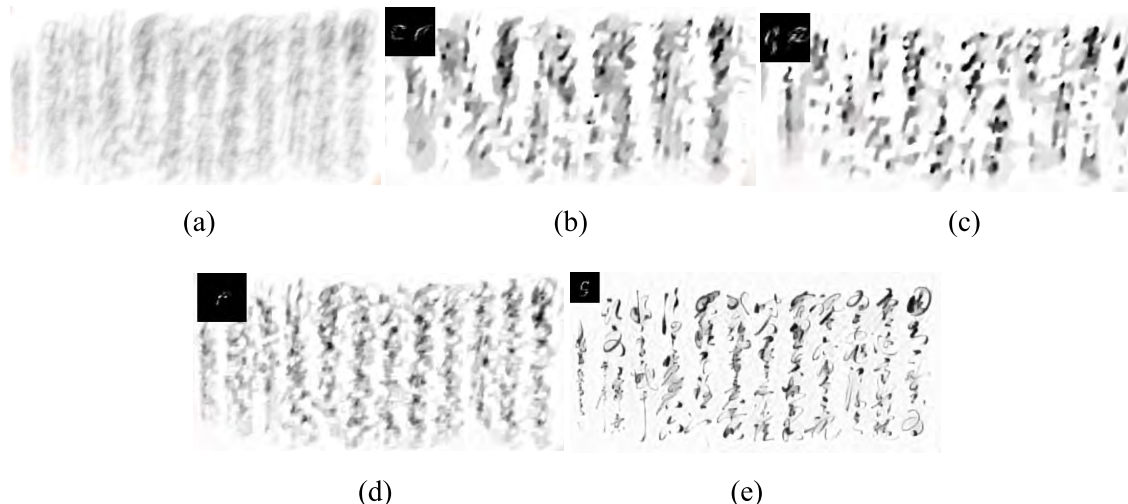


**FIGURE 13.** Visual comparisons of state-of-the-art methods on a text blurry image. (a) Blurry image; (b) Xu [4]; (c) Pan [32]; (d) Pan [5]; (e) Proposed. (Best viewed on high-resolution display with zoom-in).

## IV. MODEL ANALYSIS

### A. EFFECTIVENESS OF THE PROPOSED REGULARIZER

Our method without the enhancing component reduces to the  $L_0$  gradient prior [4]. To demonstrate the effectiveness of the proposed regularizer, we remove the enhancing component from our implementation, i.e., we replace the proposed prior

with  $L_0$  gradient prior. Fig. 6 shows the test blurry image, the intermediate latent image and the deblurred results. Compared with the  $L_0$  gradient prior, the smoothing-enhancing regularizer generate more high contrast structures, guiding the model to estimate the accurate kernel. We also compared our regularizer with the dark channel prior based method.



**FIGURE 14.** Visual comparisons of state-of-the-art methods on a face blurry image. (a) Blurry image; (b) Pan [36]; (c) Xu [4]; (d) Proposed. (Best viewed on high-resolution display with zoom-in).

As shown in Fig. 6, though the dark channel prior enhances the strong edges, it also generates false edges in the smooth region, leading to inaccurate kernel estimation. In contrast, our regularizer doesn't have this problem.

#### B. RELATION WITH EXPLICIT EDGE SELECTION METHODS

Explicit edge selection methods usually employ ad-hoc operators such as the shock filter to enhance step-like edges. The shock filter renders all selected strong edges step-like, which does not always hold for real images. In contrast, the proposed regularizer adaptively enhances strong edges based on the gradient magnitude, resulting in more reliable results. Moreover, the proposed model inherently incorporates strong edge selection and enhancement into one objective, hence it does not encounter the edge location problem, which is inherent in the shock filter.

#### C. EXTENSIONS TO OTHER SPECIFIC SCENARIOS

As the proposed regularizer enhances the strong edges, it can be directly applied to specific scenarios such as deblurring text images and face images. For this kinds of images, the enhanced strong edges act as the exemplar that helps to accurately estimate the kernels.

Low illumination image deblurring is particularly challenging because the blurred image often lacks strong edges and contains saturated pixels. However, as shown in [37], saturated pixels may record the trajectory of the camera, which has the similar shape of the kernel. Thus we use the large  $\lambda$  (typically 1.5) and small  $\beta$  (typically 2) to smooth out all insignificant edges from the blurred image and aggressively enhance the saturated pixels. Note that we keep  $\lambda$  fixed during the computation for this type of images. Combining

**TABLE 1.** Running time (seconds) of different methods.

Method	255 × 255	800 × 800
Pan [5] (Matlab)	83.74	1265.32
Yan [20] (Matlab)	166.79	1632.12
Li [18] (Matlab)	71.58	554.24
Ours (Matlab)	8.76	36.40

the fidelity term and the enhancing property of the proposed regularizer, the saturated area would be enhanced as the dot-like pattern, as shown in Fig. 7. We present more low-light deblurring results in Section V.

#### D. CONVERGENCE PROPERTY

Fig. 8 shows the loss and kernel similarity w.r.t the number of iterations, which suggests that the proposed method converges after less than fifty iterations. Thus, we can adopt the stopping criteria by setting a threshold  $\tau$  for the absolute value of the loss differences of adjacent iterations, i.e.,  $|E^i - E^{i-1}| < \tau$ . In practice, however, we find five iterations for both the latent image and kernel estimation at one image level are enough. Thus in this paper we empirically set the max iteration per scale to 5 as a trade-off between accuracy and speed.

#### E. COMPUTATIONAL COMPLEXITY

We compare the running time of three leading deblurring methods and the results are shown in table 1. All the experiments are conducted on the same PC with an Intel i7 CPU and 8GB memory. Dark channel [5] and extreme channel [20] priors require to compute the dark channel, bright channel and look-up tables with running windows of size  $k$  (typically 32), which have the computational complexity  $O(k^2N)$ , where  $N$  is the number of pixels. The discriminative prior [18] uses the CNN to learn the prior as the binary classifier, while CNN is computationally expensive, which has  $O(k^2CLN)$  computational complexity, where  $k$ ,  $C$ ,  $L$  and  $N$  are the kernel size, number of kernels, number of layers and number of pixels of feature maps. In contrast, the proposed regularizer is computationally efficient, which has  $O(N)$  computational complexity, leading to more than  $10\times$  faster execution time. Our method can be further sped up using GPU acceleration.

#### V. EXPERIMENTAL RESULTS

We show results of our algorithm in comparison with other state-of-the-art deblurring methods [1]–[5], [9], [17], [18], [20], [37]. We first test our method on two publicly available blur image datasets [11], [35] and compare the results with other state-of-the-art blind restoration methods. We then test our method using real natural images. Finally, we extend our comparisons to text, face and low-illumination images. For fairness, we use the non-blind deblurring algorithm [32] for natural, text and face images and use [37] for low illumination images.

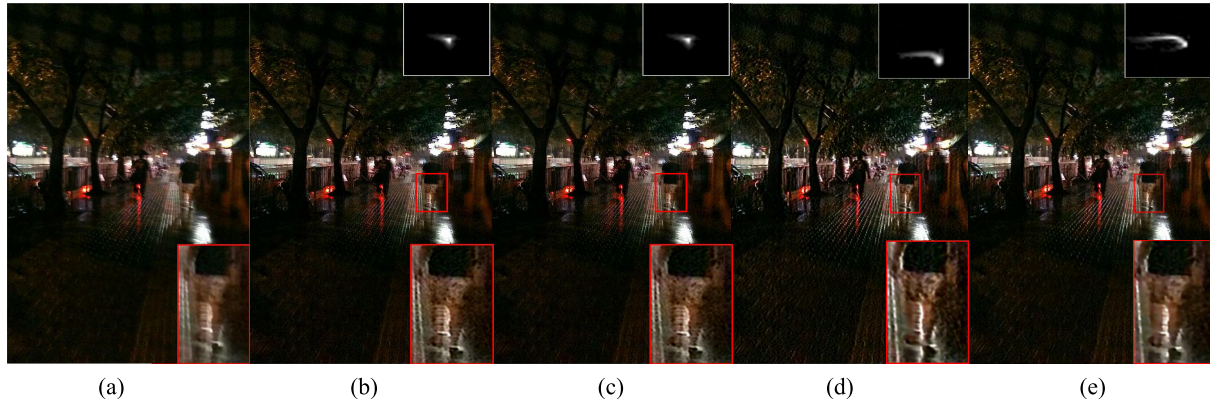


**FIGURE 15.** Visual comparisons of state-of-the-art methods on a low illumination image. (a) Blurry image; (b) Pan [5]; (c) Pan [32]; (d) Hu [37]; (e) Proposed. (Best viewed on high-resolution display with zoom-in).

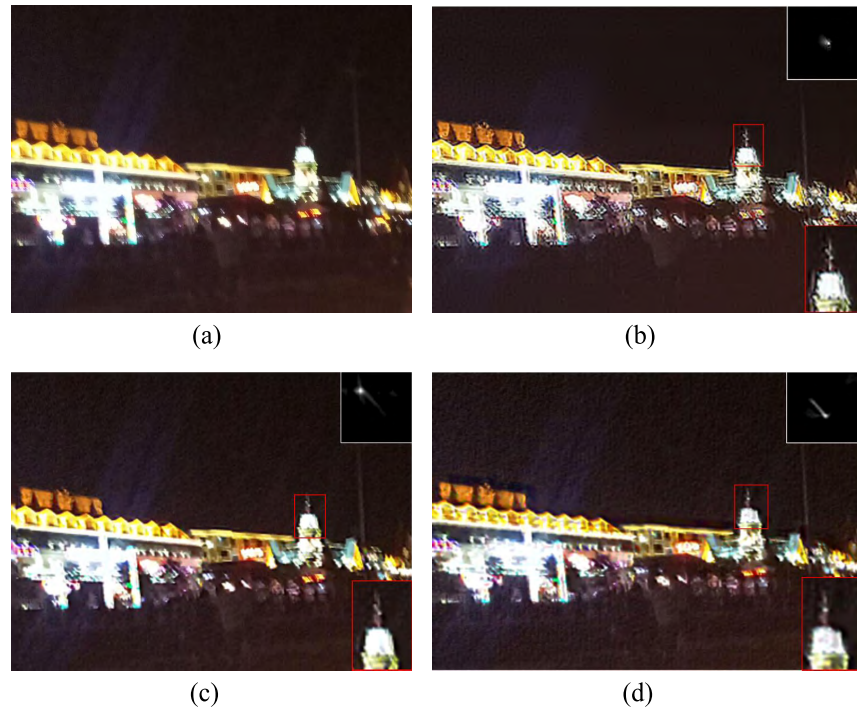


**FIGURE 16.** Visual comparisons of state-of-the-art methods on a low illumination image. (a) Blurry image; (b) Pan [5]; (c) Hu [37]; (d) Proposed. (Best viewed on high-resolution display with zoom-in).

#### A. PARAMETER SELECTION

There are five parameters in the model,  $\alpha$ ,  $\beta$ ,  $\varepsilon$ ,  $\lambda$  and  $\gamma$ .  $\alpha$  and  $\gamma$  balance the weight between the fidelity term and the regularizer for the latent image and kernel respectively,  $\beta$  and  $\varepsilon$  control the enhancement degree of the strong edge, and  $\lambda$  is the smoothing threshold. Among these parameters,  $\beta$  and  $\lambda$  are relative sensitive to kernel size. Keeping the other parameters fixed, smaller  $\beta$  results in sharper edges and larger  $\lambda$  smooths more structures. Since blur images with relatively large kernels often have less reliable edges than those with relatively small kernels, we use large  $\lambda$  (typically 1.5) and small  $\beta$  (typically 2) for large kernels and small  $\lambda$  (typically

0.5) and large  $\beta$  (typically 10) for slight or moderate blur. We set  $\alpha = \varepsilon = 0.001$  and  $\gamma = 2$  in most of the experiments.

#### B. NATURAL IMAGES

We first tested the algorithm on dataset [11], which contains 32 blurred images of size  $255 \times 255$  each with eight kernels ranging in size from  $13 \times 13$  to  $27 \times 27$ . We compared our algorithm with those proposed in [1]–[5], [9], [20]. Fig. 9 shows the cumulative histograms of the error ratios for the eight algorithms. The results of our algorithm are competitive with those of the leading algorithms [5], [20].

We then evaluated our method using dataset [35], which contains four natural images and twelve blur kernels ranging in size from small to large. PSNR was computed by comparing each images with 199 clear images captured along the camera motion trajectory. As shown in Fig. 10, our method is consistently competitive with the leading methods [5], [20] and [18]. Fig. 11 shows the results obtained on one challenging image with heavy blur in the dataset. Our method recovers more abundant details (e.g. the numbers under the dial plate). We further compared the model performances using an outdoor image, as shown in Fig. 12. Comparing with other leading algorithms, our algorithm recovers more details.

### C. TEXT IMAGES

We further evaluated the proposed method using text images. Fig. 13 shows one challenging example without gamma correction. While method in [5] and [32] failed, our model recovers visually pleasant results.

### D. FACE IMAGES

Blurred face images are also challenging for most deblurring methods, as they contain fewer strong edges or structures. We used a real blurred face image to test our algorithm, as shown in Fig. 14. Our method recovers the clearer image with fewer artifacts compared with [36], which explicitly extracts facial structures using exemplar datasets.

### E. LOW ILLUMINATION IMAGES

Low illumination blurred images are particularly challenging for most deblurring methods, as they often suffer from saturation effects that can ruin the algorithm in the kernel estimation procedure. As shown in Fig. 15, the recovered image by our algorithm is visually competitive with that obtained by [37] (see the zoomed-in area), which is tailored to deblur low illumination images, whereas the kernel estimated by [5] and [32] appeared to be like a delta function. Fig. 16 shows a more challenging example, which is difficult to extract the kernel from the light strikes. While all the compared models fail, the proposed model recovers the clearer image, e.g., the top of the tower. These examples demonstrate the effectiveness of the proposed algorithm for low illumination images.

## VI. DISCUSSION

While the proposed regularizer (2) appears similar to the following regularizer, they have significant differences:

$$\min_u : \phi(u) = \int \frac{1}{D + \varepsilon} dx dy \quad (24)$$

where  $\varepsilon$  is a small constant. The key difference between (2) and (24) is that (24) enhances all elements in images including noise, whereas (2) enhances only strong edges based on  $\varepsilon$ . The associated heat flow of (24) is

$$\frac{\partial \phi}{\partial t} = \nabla \cdot \left( \frac{-1}{(D + \varepsilon)^2 D} \nabla u \right) \quad (25)$$

We see that the diffusion coefficient is always negative, suggesting that all the elements including noise will be enhanced during computation.

## VII. CONCLUSION

In this paper, we proposed the smoothing-enhancing regularizer for image deblurring. The motivation came from the fact that the success of recent priors mainly stemmed from their properties, which implicitly generated an unnatural latent image suppressing insignificant structures and preserving only salient edges. These salient edges guided the models to estimate an accurate kernel. The proposed regularizer not only removed the harmful subtle image structures but also enhanced the high contrast ones of the unnatural latent images. Different from most of existing methods which only smoothed the subtle structures of latent images, our approach elegantly incorporated the smoothing and enhancing operations into one regularizer. Compared with explicit strong edge-selection methods which usually used local shock filter to enhance the strong edges, our strong edges were selected and adaptively enhanced without filtering in extra steps.

The proposed regularizer was challenging to optimize owing to its highly nonlinear nature. We thus derived a fast optimization scheme based on half-quadratic splitting and fixed-point iteration scheme. The optimization scheme was quick because it only required a few additional shrinkage operations compared with the original half-quadratic splitting algorithm. Owing to the high efficiency of the optimization scheme, the proposed method was much more efficient than the recent leading algorithms, with up to more than  $10\times$  faster execution time. The proposed algorithm archived the state of the art results on natural deblurring natural images and could be extended to other challenging deblurring tasks, such as text, face, and low illuminated images.

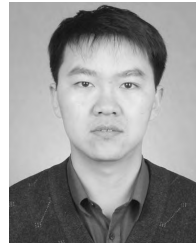
## REFERENCES

- [1] S. Cho and S. Lee, "Fast motion deblurring," *ACM Trans. Graph.*, vol. 28, no. 5, p. 145, 2009.
- [2] D. Krishnan, T. Tay, and R. Fergus, "Blind deconvolution using a normalized sparsity measure," in *Proc. IEEE Conf. Comput. Vis. Pattern Recognit. (CVPR)*, Jun. 2011, pp. 233–240.
- [3] Q. Shan, J. Jia, and A. Agarwala, "High-quality motion deblurring from a single image," *ACM Trans. Graph.*, vol. 27, no. 3, p. 73, 2008.
- [4] L. Xu, S. Zheng, and J. Jia, "Unnatural L0 sparse representation for natural image deblurring," in *Proc. IEEE Conf. Comput. Vis. Pattern Recognit.*, Jun. 2013, pp. 1107–1114.
- [5] J. Pan, D. Sun, H. Pfister, and M.-H. Yang, "Blind image deblurring using dark channel prior," in *Proc. IEEE Conf. Comput. Vis. Pattern Recognit.*, Jun. 2016, pp. 1628–1636.
- [6] P. Cui, S. Liu, and W. Zhu, "General knowledge embedded image representation learning," *IEEE Trans. Multimedia*, vol. 20, no. 1, pp. 198–207, Jan. 2018.
- [7] X. Liu, W. Liu, T. Mei, and H. Ma, "PROVID: Progressive and multimodal vehicle reidentification for large-scale urban surveillance," *IEEE Trans. Multimedia*, vol. 20, no. 3, pp. 645–658, Mar. 2018.
- [8] A. Levin and Y. Weiss, "User assisted separation of reflections from a single image using a sparsity prior," *IEEE Trans. Pattern Anal. Mach. Intell.*, vol. 29, no. 9, pp. 1647–1654, Sep. 2007.
- [9] R. Fergus, B. Singh, A. Hertzmann, S. T. Roweis, and W. T. Freeman, "Removing camera shake from a single photograph," *ACM Trans. Graph.*, vol. 25, no. 3, pp. 787–794, 2006.

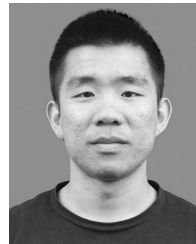
- [10] A. Levin, Y. Weiss, F. Durand, and W. T. Freeman, "Efficient marginal likelihood optimization in blind deconvolution," in *Proc. IEEE Conf. Comput. Vis. Pattern Recognit. (CVPR)*, Jun. 2011, pp. 2657–2664.
- [11] A. Levin, Y. Weiss, F. Durand, and W. T. Freeman, "Understanding and evaluating blind deconvolution algorithms," in *Proc. IEEE Conf. Comput. Vis. Pattern Recognit.*, Jun. 2009, pp. 1964–1971.
- [12] L. Xu and J. Jia, "Two-phase kernel estimation for robust motion deblurring," in *Proc. Eur. Conf. Comput. Vis.* Berlin, Germany: Springer, 2010, pp. 157–170.
- [13] S. Cho, J. Wang, and S. Lee, "Handling outliers in non-blind image deconvolution," in *Proc. IEEE Int. Conf. Comput. Vis. (ICCV)*, Nov. 2011, pp. 495–502.
- [14] N. Joshi, R. Szeliski, and D. J. Kriegman, "PSF estimation using sharp edge prediction," in *Proc. IEEE Conf. Comput. Vis. Pattern Recognit. (CVPR)*, Jun. 2008, pp. 1–8.
- [15] L. Sun, S. Cho, J. Wang, and J. Hays, "Edge-based blur kernel estimation using patch priors," in *Proc. IEEE Int. Conf. Comput. Photogr. (ICCP)*, Apr. 2013, pp. 1–8.
- [16] T. Michaeli and M. Irani, "Blind deblurring using internal patch recurrence," in *Proc. Eur. Conf. Comput. Vis.* Cham, Switzerland: Springer, 2014, pp. 783–798.
- [17] J. Pan, W. Ren, Z. Hu, and M.-H. Yang, "Learning to deblur images with exemplars," *IEEE Trans. Pattern Anal. Mach. Intell.*, vol. 41, no. 6, pp. 1412–1425, Jun. 2019.
- [18] L. Li, J. Pan, W.-S. Lai, C. Gao, N. Sang, and M.-H. Yang, "Learning a discriminative prior for blind image deblurring," in *Proc. IEEE Conf. Comput. Vis. Pattern Recognit.*, Jun. 2018, pp. 6616–6625.
- [19] J. H. Money and S. H. Kang, "Total variation minimizing blind deconvolution with shock filter reference," *Image Vis. Comput.*, vol. 26, no. 2, pp. 302–314, 2008.
- [20] Y. Yan, W. Ren, Y. Guo, R. Wang, and X. Cao, "Image deblurring via extreme channels prior," in *Proc. IEEE Conf. Comput. Vis. Pattern Recognit.*, Jul. 2017, vol. 2, no. 5, pp. 4003–4011.
- [21] Y. Bai, H. Jia, M. Jiang, X. Liu, X. Xie, and W. Gao, "Single image blind deblurring using multi-scale latent structure prior," *IEEE Trans. Circuits Syst. Video Technol.*, to be published.
- [22] Y. Bai, G. Cheung, X. Liu, and W. Gao, "Graph-based blind image deblurring from a single photograph," *IEEE Trans. Image Process.*, vol. 28, no. 3, pp. 1404–1418, Mar. 2019.
- [23] M. Ljubenović and M. A. T. Figueiredo, "Blind image deblurring using class-adapted image priors," in *Proc. IEEE Int. Conf. Image Process. (ICIP)*, Sep. 2017, pp. 490–494.
- [24] M. Hradiš, J. Kotera, P. Zemcik, and F. Šroubek, "Convolutional neural networks for direct text deblurring," in *Proc. BMVC*, vol. 10, 2015, pp. 1–13.
- [25] C. J. Schuler, M. Hirsch, S. Harmeling, and B. Schölkopf, "Learning to deblur," *IEEE Trans. Pattern Anal. Mach. Intell.*, vol. 38, no. 7, pp. 1439–1451, Jul. 2016.
- [26] A. Chakrabarti, "A neural approach to blind motion deblurring," in *Proc. Eur. Conf. Comput. Vis.* Cham, Switzerland: Springer, 2016, pp. 221–235.
- [27] S. A. Bigdeli, M. Zwicker, P. Favaro, and M. Jin, "Deep mean-shift priors for image restoration," in *Proc. Adv. Neural Inf. Process. Syst.*, 2017, pp. 763–772.
- [28] K. Schelten, S. Nowozin, J. Jancsary, C. Rother, and S. Roth, "Interleaved regression tree field cascades for blind image deconvolution," in *Proc. IEEE Winter Conf. Appl. Comput. Vis. (WACV)*, Jan. 2015, pp. 494–501.
- [29] T. F. Chan and C.-K. Wong, "Total variation blind deconvolution," *IEEE Trans. Image Process.*, vol. 7, no. 3, pp. 370–375, Mar. 1998.
- [30] Z. Dou, M. Song, K. Gao, and Z. Jiang, "Image smoothing via truncated total variation," *IEEE Access*, vol. 5, pp. 27337–27344, 2017.
- [31] E. Esser, L. Guasch, T. van Leeuwen, A. Y. Aravkin, and F. J. Herrmann, "Total variation regularization strategies in full-waveform inversion," *SIAM J. Imag. Sci.*, vol. 11, no. 1, pp. 376–406, 2016.
- [32] J. Pan, Z. Hu, Z. Su, and M.-H. Yang, "Deblurring text images via L0-regularized intensity and gradient prior," in *Proc. IEEE Conf. Comput. Vis. Pattern Recognit.*, Jun. 2014, pp. 2901–2908.
- [33] C. Wang, L. Sun, Z. Chen, J. Zhang, and S. Yang, "Multi-scale blind motion deblurring using local minimum," *Inverse Problems*, vol. 26, no. 1, Jan. 2010, Art. no. 015003.
- [34] D. Zoran and Y. Weiss, "From learning models of natural image patches to whole image restoration," in *Proc. Int. Conf. Comput. Vis. (ICCV)*, 2011, pp. 479–486.
- [35] R. Köhler, M. Hirsch, B. Mohler, B. Schölkopf, and S. Harmeling, "Recording and playback of camera shake: Benchmarking blind deconvolution with a real-world database," in *Proc. Eur. Conf. Comput. Vis.* Berlin, Germany: Springer, 2012, pp. 27–40.
- [36] J. Pan, Z. Hu, Z. Su, and M.-H. Yang, "Deblurring face images with exemplars," in *Proc. Eur. Conf. Comput. Vis.* Cham, Switzerland: Springer, 2014, pp. 47–62.
- [37] Z. Hu, S. Cho, J. Wang, and M.-H. Yang, "Deblurring low-light images with light streaks," in *Proc. IEEE Conf. Comput. Vis. Pattern Recognit.*, Jun. 2014, pp. 3382–3389.
- [38] B. Wahlberg, S. Boyd, M. Annergren, and Y. Wang, "An ADMM algorithm for a class of total variation regularized estimation problems," 2012, *arXiv:1203.1828*. [Online]. Available: <https://arxiv.org/abs/1203.1828>
- [39] T. Goldstein and S. Osher, "The split Bregman method for L1-regularized problems," *SIAM J. Imag. Sci.*, vol. 2, no. 2, pp. 323–343, 2009.



**ZEYANG DOU** received the B.E. degree in mathematics from Baoding University, China, in 2012, and the M.S. degree in computational mathematics from the Communication University of China, in 2016. He is currently pursuing the Ph.D. degree with the Beijing Institute of Technology. His research interests include image processing, machine learning, and deep learning.



**KUN GAO** received the B.A. degree in electrical engineering and the Ph.D. degree in instrument science and engineering from Zhejiang University, China, in 1995 and 2002, respectively. From 2002 to 2004, he was a Postdoctoral Fellow with Tsinghua University, China. Since 2005, he has been with the Beijing Institute of Technology, China, where he is involved in infrared technology and real-time image processing. He is a member of the Optical Society of China.



**XIAODIAN ZHANG** received the B.E. degree in opto-electronics information science and engineering with the Beijing Institute of Technology, in 2018, where he is currently pursuing the M.S. degree in optical engineering with the School of Optoelectronics. His current research interests include deep learning, and object detection in natural and remote sensing scene.



**HONG WANG** received the B.E. degree in electronic science and technology from Dezhou University, China, in 2014, and the M.S. degree in electronic circuit and system from Tianjin Normal University, China, in 2018. She is currently pursuing the Ph.D. degree with the Beijing Institute of Technology. Her research interests include image processing, pattern recognition, machine learning, and deep learning.